Characterization of an Acousto-optic Tunable Filter and Use in Visible Spectrophotometry

EWA G. BUCHER and JON W. CARNAHAN*

Department of Chemistry and Biochemistry, Northern Illinois University, DeKalb, Illinois 60115

The use of a paratellurite acousto-optic tunable filter (AOTF) is demonstrated as a monochromator for spectrophotometry. This device operates in the range of 400 to 700 nm with a resolution from 2.5 nm (at 633 nm) to 0.5 nm (at 400 nm). Results of the initial characterizations indicate that behavior follows the theoretical model in terms of frequency/wavelength relationships, dependence of the output wavelength upon the incident radiation angle, and bandpass as a function of wavelength. Initial results of spectroscopic characterizations of permanganate, cobalt(II), holmium(III), praseodymium(III), and neodymium(III) solutions are presented. Placing a polarizer in the light path reduced the amount of stray light reaching the detector. Two types of photomultiplier tubes were used as detectors. The sensitivity of the PMTs varied at different wavelengths, which affected spectral responses and the effects of scattered light.

Index Headings: **Visible spectroscopy; Acousto-optic tunable filter.**

INTRODUCTION

An acousto-optic tunable filter (AOTF) is a device that operates on the basis of the interaction between optical radiation and a compression or shear wave traveling within an anisotropic material at a near-acoustic velocity. The device is typically made of an optically transparent material in which the compression wave is generated by an attached piezoelectric transducer. The frequency of compression wave application is typically in the tens to hundreds of megahertz range. Interaction between light and the compression wave allows light in a very narrow wavelength range to be transmitted. The wavelength output is governed by the applied frequency. In essence, an AOTF functions as a tunable, variable-wavelength, transmissive filter. This characteristic offers potential use as a monochromator for spectrophotometry. Details concerning AOTF theory may be found elsewhere.[1–5]

Using an AOTF as a wavelength selection device has several advantages. These devices are small and relatively inexpensive. As AOTFs are solid state, there are no moving parts. Spectral resolution is comparable to that of moderate-resolution prism- and grating-based spectrophotometers. Because the frequency of the applied acoustic wave can be changed on the microsecond time scale, the device has rapid wavelength access capabilities. Random or sequential wavelength selection is possible. These characteristics prompt examinations of AOTFs for spectrophotometry.

The wavelength of light undergoing AOTF diffraction (λ), and thus transmission, is described by the equation[1]

$$\lambda = \frac{v\Delta n}{f}\sqrt{\sin^4\Theta_i + \sin^2 2\Theta_i} \qquad (1)$$

where v is the acoustic velocity, f is the frequency of the applied acoustic wave, and Θ_i is the angle of incidence. The parameter Δn is the difference in the refractive indices for the incident and diffracted radiation. Radiation that undergoes AOTF diffraction experiences a 90° polarization rotation and may exit the material at a different angle from that for the incident radiation. Another important parameter, the bandpass of the diffracted light, depends on the wavelength of the diffracted light. The full width at half-maximum (FWHM), $\Delta\lambda$, is expressed by the following equation:

$$\Delta\lambda = \frac{0.9\lambda^2}{\Delta n L \sin^2\Theta_i}. \qquad (2)$$

All terms were previously defined except for L, which is the interaction length between the acoustic wave and optical radiation. If all other terms are assumed to be approximately constant, $\Delta\lambda$ is proportional to the square of the wavelength. This relationship dictates that better resolution should occur at shorter wavelengths.

The useful optical range of an acousto-optic device is determined by the material used for the construction of a device. Several additional characteristics such as acousto-optic figures of merit, uniformity, light scattering, mechanical properties, and cost also must be taken into account.[5] Currently, for the infrared spectral region, thallium arsenic selenite (Tl_3AsSe_3) is the material of choice. Mercurous chloride (Hg_2Cl_2) has been used for the 0.4 to 20 μm region. For the visible range to about 4 μm, lithium niobate ($LiNbO_3$), calcium molybdate ($CaMoO_4$), and tellurium dioxide (TeO_2) have found applications. Quartz is the material most commonly used for the ultraviolet spectral region.

There have been several reports on the application of acousto-optic devices to different types of spectroscopy. Fulton and Horlick[8] examined paratellurite AOTF applications to atomic spectroscopy with hollow cathode lamps and the inductively coupled plasmas (ICPs). With two AOTF devices they were able to successfully monitor the spectral region from 350 to 650 nm. A paratellurite AOTF, combined with a fiber-optic Fabry–Perot interferometer, was used to construct a high-resolution spectrometer.[7] The resolution of the system approached that of a 1.5 m spectrometer. This device was applied to the ICP determination of uranium isotopes (U-235 and U-238). A quartz AOTF was used as a detector for HPLC[6] to obtain 250 to 650 nm spectra of separated chlorophenols. Tran et al. applied acousto-optic tunable filters to fluorescence spectroscopy.[9–11] These workers took advantage of the ability of a multiple acoustic frequency input device to provide multiple-wavelength excitation. A second AOTF was used for multiwavelength emission

Received 31 January 1998; accepted 4 January 1999.

* Author to whom correspondence should be sent.

0003-7028/99/5305-0603$2.00/0

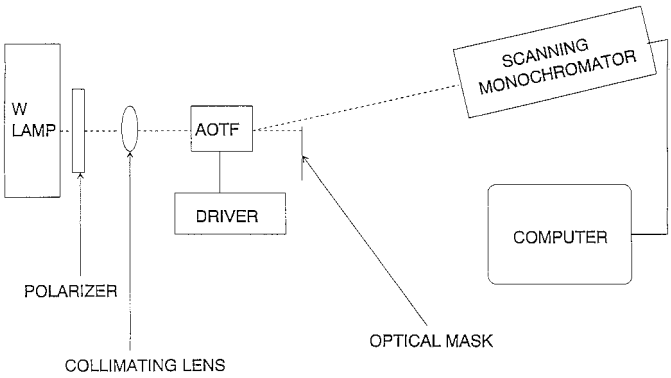

FIG. 1. System for initial characterization of the AOTF.

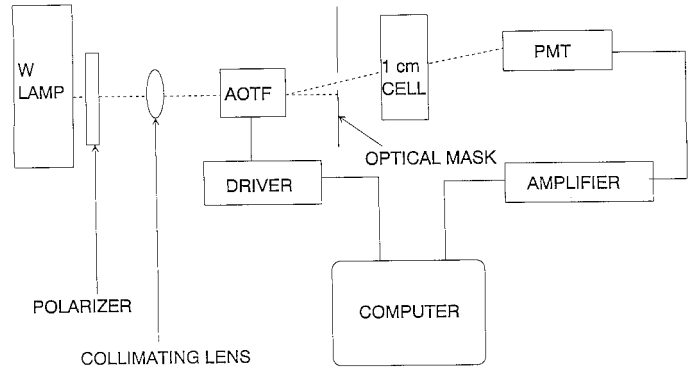

FIG. 2. Visible AOTF spectrophotometer.

monitoring. The ability of an AOTF to rapidly change the diffracted wavelength made it possible to register the whole fluorescence spectrum in a flow injection analysis stream.[9]

Acousto-optic tunable filters have also found use in Raman and near-infrared spectroscopies. An AOTF, combined with krypton laser (647 nm excitation), holographic Raman filters, and photon-counting silicon avalanche photodiode detection, was used to construct a miniaturized Raman spectrometer of moderate resolution.[12] The ability of multiple-frequency AOTFs to simultaneously diffract radiation of several wavelengths was utilized in the construction a near-infrared Hadamard transform spectrophotometer.[14] As many as 20 radio-frequency (rf) signals were injected into the AOTF without producing artifacts. However, compromises between radiation throughput and spectral resolution were required. In another application, an AOTF was used as a part of a near-infrared spectrophotometer with a europium-doped fiber amplifier as a light source.[13] The combination of these two devices allowed the construction of an instrument in which common near-infrared spectroscopy limitations of speed, stability, and light throughput were reduced. The sensitivity of the instrument was comparable to the sensitivity of a halogen–tungsten lamp AOTF spectrophotometer, but with approximately 20 times greater light intensity than the traditional 250 W halogen–tungsten lamp. A charge-coupled device (CCD)/AOTF system was used to image systems in the visible and near-infrared spectral regions,[16] as well as for Raman imaging spectroscopy.[15] A similar system with a fiber optic was used for remote monitoring of a number of analytes.[17]

While AOTF devices have been utilized for numerous applications in a variety of spectroscopic techniques, comprehensive characterizations of important spectroscopic characteristics including linearity, stray light, resolution, etc., are lacking. In this paper, the application of an AOTF device to visible spectrophotometry is detailed. The spectroscopic behavior of the AOTF was first characterized. The relationships between the applied acoustic frequency, incident angle, applied power, spectral bandpass, and wavelength of the diffracted light were determined in terms of spectrophotometer suitability. With this information, an AOTF spectrophotometer was constructed. Wavelength calibration was accomplished. Absorption spectra and calibration plots for several species were obtained. Effects of stray radiation and detector response and their effects on calibrations and spectral information are highlighted.

EXPERIMENTAL

The paratellurite AOTF used in this study was purchased from IntraAction Corp. (Model ATF-1102BPJ1). The device has a spectral range of 400 to 700 nm and an optical aperture of 3 × 3 mm. The driver frequency is controlled through a frequency synthesizer (75 to 150 MHz, 10 kHz resolution, 10 W maximum; Model VFE-1004C4, IntraAction Corp).

AOTF Characterization. The system used for the initial characterization is shown in Fig. 1. A tungsten lamp (GCA McPherson EU-701-50) directed through a 1 mm diameter aperture was used as the light source. The radiation passed through a removable dichroic sheet polarizer, a 5 cm focal length collimating lens (f/2), and to the AOTF device. Ray tracing was utilized to calculate that the maximum deviation from collimation was slightly less than 1°, far less than the manufacturer's maximum estimated acceptance angle of 4.2°. The combination of the AOTF 3 × 3 mm square aperture and collimated radiation avoided the problem of radiation reflecting from the internal side walls of the AOTF. An optical mask was placed in the optical path after the AOTF to isolate the desired diffracted radiation. Diffracted light was directed to a Spex 1000M 1 m monochromator (Spex Industries). The monochromator had a 2400 grooves/mm grating blazed at 500 nm, and the slits were set to 50 μm; the spectrometer had a spectral bandpass of 0.04 nm. The resolution of the monochromator was far better than the resolution of the AOTF device and did not influence the measurements of the AOTF characteristics. The output from the monochromator was directed to a 486 microcomputer equipped with AutoScan software (Version 1.1). Measurements of the angle of the incident light were obtained by determining the angle of the reflection of the He laser.

AOTF Spectrophotometer. The AOTF device was utilized for spectrophotometry monochromation, as shown in Fig. 2. Tungsten lamp radiation was directed through the sheet polarizer and the 5 cm focal length collimating lens to the AOTF device. A 2 mm diameter optical mask was used to reduce effects of nondiffracted radiation. Diffracted light was passed through a 1 cm pathlength quartz spectrophotometry cell and was detected by a photomultiplier tube. Two different photo-

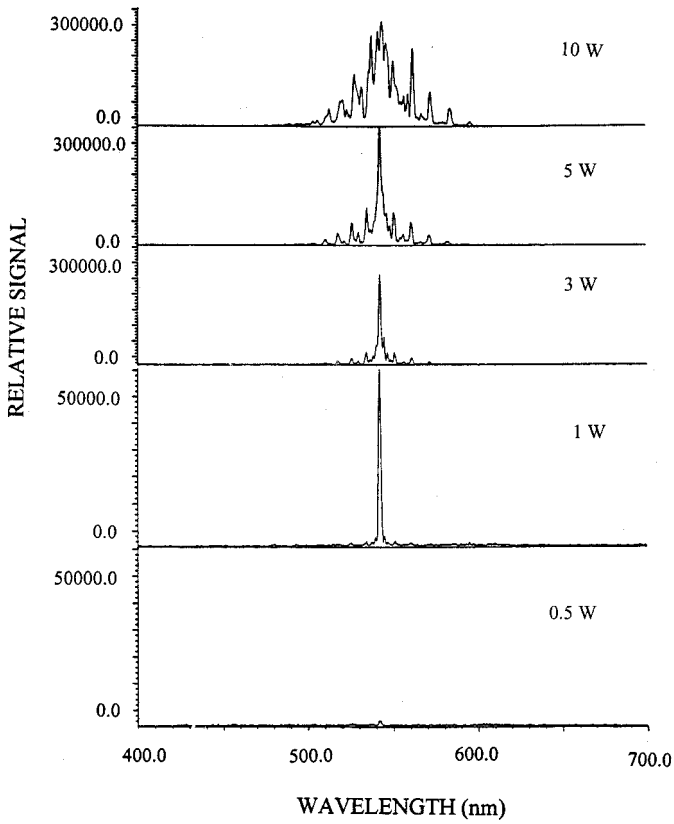

FIG. 3. Effects of applied power upon AOTF output.

multiplier tubes were utilized; they were types 1P28 and R955 (Hamamatsu Photonics KK). The voltages of the photomultiplier tube were maintained by a GCA Pherson Model EU-701-30 power supply/housing at 700 V for the 1P28 PMT and at 800 V for the R955 PMT. The PMT currents were converted to voltages, and the signals were filtered with a 0.01 s time constant filter by an NIU-constructed operational amplifier-based system. A 486 computer with a Lab View program (Lab View 4.0, National Instruments) and SCXI-1300 interface driver board (National Instruments) were used to control the AOTF and acquire spectral data. The spectra were acquired by scanning the 75 to 150 MHz range in 0.19 MHz increments, which yielded 400 data points per spectrum. Each of the 400 spectral data points represented the average of 100 readings. The PMT output was read with an analog-to-digital acquisition rate of 1000 scans/s. An entire spectrum was recorded within 1 min (141 ms/point for each of the 400 points). Hitachi U-3410 and Varian 2290 UV-vis spectrophotometers were used to obtain spectral comparisons.

RESULTS AND DISCUSSION

Initial Characterization of the AOTF. *Power Optimization.* The system described in Fig. 1 was used to characterize the spectral characteristics of the diffracted light at different powers applied to the AOTF device. The measurements were performed with the AOTF driver set at 100 MHz, and the power was increased in increments from 0 to 10 W. Representative spectra recorded under these conditions are presented in Fig. 3.

Although a feature clearly appears at 542 nm, it is difficult to distinguish the diffracted light from the background noise when 0.5 W is applied. At 1 W, this peak at 542 nm becomes intense and is relatively symmetric. When the power is increased to 3 W, the intensity of the peak increases more than fourfold. However, a significant amount of radiation exits the AOTF, which is centered at, but is several nanometers from, the 542 nm central feature. This trend is accentuated at 5 W. When 10 W is applied, a broad spectral feature covering a 100 nm range appears.

Theoretically, the intensity of the diffracted light should be directly proportional to the applied rf power. Tran and Furlan[11] studied this relationship for their paratellurite AOTF at two different frequencies corresponding to 514.5 and 488 nm and determined that the relationship was linear over four orders of magnitude from 0.01 to over 10 mW. In our experiments, as we operated at much higher powers, the intensities of the peaks linearly increased with the applied power only in the lower range. At high powers a significant amount of the radiation is diffracted at wavelengths away from the central peak. Similar effects were observed by Turner and Treado,[14] who also had to compromise the throughput of their TeO_2 AOTF because of the light outside the FWHM. It is likely that these higher power effects are induced by spurious reflections of compression waves from the crystal walls.

We repeated the same experiment at two additional frequencies (86 and 130 MHz) with similar results. At these frequencies the optimum spectrum was recorded at 1.5 W. The power of 1.5 W was therefore chosen for the remainder of the experiments.

Output Radiation Wavelength-Intensity Profile. Theoretically, the wavelength-intensity relationship of the AOTF output should correspond to a sinc^2 function, with characteristic side lobes. A detailed sample spectrum, obtained at 86 MHz and 1.5 W, is shown in Fig. 4. The shape of our spectrum follows the theoretical model. Integration of the peak areas indicates that 92.8% of the radiation appears at the peak of maximum intensity. The areas of the first and second side lobes account for 4.4 and 2.8%, respectively. These values are in close agreement with the theoretical value of 7% transmission outside the main peak. It should be noted that this small amount of "nonmonochromatic" light in the side lobes may increase the effective amount of stray light in spectrophotometric experiments.

Frequency/Wavelength Relationship. To experimentally establish frequency/wavelength relationships for our device, we registered AOTF spectra at various driver frequencies by using the system shown in Fig. 1. The relationship between the AOTF output wavelength and the applied acoustic frequency is described in Eq. 1. On the basis of this relationship, it can be expected that acoustic waves of higher frequency will diffract light of lower wavelength, and indeed this is the effect observed in our experiments.

The acoustic velocity (v) in a given crystalline material is constant. If it is assumed that the differences between the refractive indices of the incident and diffracted light do not change, and the angle of incident light is kept constant, Eq. 1 can be simplified to

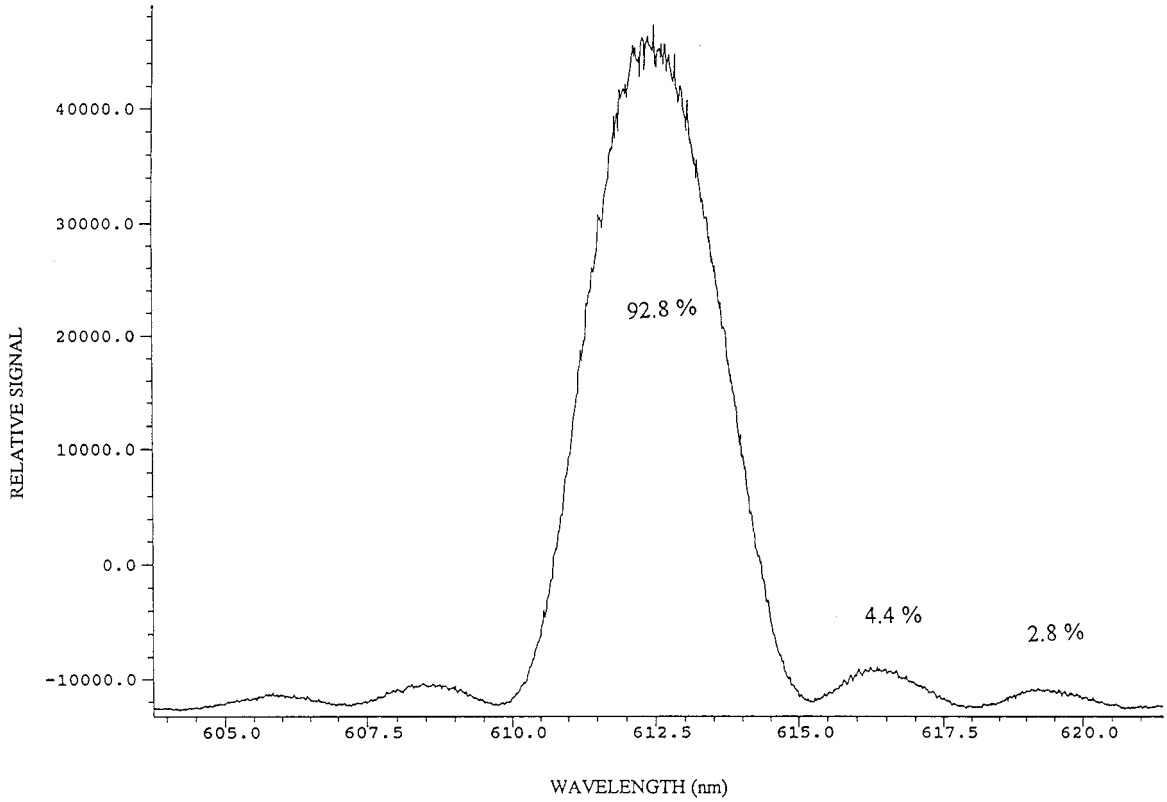

FIG. 4. Typical AOTF spectral output.

$$\lambda = \frac{c_1}{f} \tag{3}$$

where c_1 is a constant.

The frequency was increased in 15 increments in the range of 85 to 150 MHz, and the output wavelength was monitored. Results are shown in Fig. 5. The inverse frequency of 6.6×10^{-9} Hz^{-1} corresponds to 150 MHz, while the inverse frequency at 12.5×10^{-9} Hz^{-1} corresponds to 80 MHz. For these data, a first-order fit (dotted line of Fig. 5) yields an r^2 value of 0.9995. However, this plot clearly exhibits curvature. A better agreement is observed when the second-order relationship is used ($r^2 = 0.99998$). This result is shown as the solid line in Fig. 5A. Calculated uncertainties (expressed as variance) in the first- and second-order fit are shown in Fig. 5B. The variance is calculated as the square of the differences between the actual value and the value indicated by the linear fit. The second-order fit is clearly superior. The observed curvature is probably caused by the dependence of the refractive index on the optical wavelength. The value Δn in Eq. 1 represents the difference in refractive index of the ordinary and extraordinary light beam. Refractive index values are dependent upon the wavelength. The parameter $\delta n/\delta\lambda$ is greater at shorter wavelengths. The differences in the refractive indices of the ordinary and the extraordinary light will be greater at the shorter wavelengths (higher frequency) than in the longer wavelength (lower frequency) regions. This effect causes the parameter $\delta\lambda/\delta$ to be smaller at shorter wavelengths and yields the likely explanation of the curvature of Fig. 5A.

To establish the wavelength/incident angle relationship for our device, we measured the wavelength of the diffracted light while rotating the crystal over a 12° range (79° to 87°) in 14 increments. The standard deviation of the angles was 0.3°. The acoustic frequency was kept constant during the experiment at 100 MHz. Since f and ν are constant and Δn is nearly constant under these conditions, Eq. 1 reduces to

$$\lambda = c_2\sqrt{\sin^4\Theta_i + \sin^2(2\Theta_i)} \tag{4}$$

where c_2 is a constant.

Results are presented in Fig. 6. The lower end of the curve at which the sin function equals 1.003 corresponds to 87°, while the sin function value of 1.032 corresponds to 79°. The incident angle change of 8° resulted in a 17 nm variation in the wavelength output. The first-order fit yields an r^2 value of 0.994. Although the data show some scatter (likely due to the precision of the AOTF angle measurements), the results of our experiment agree well with the above theoretical equation. The variance in the wavelength of the output radiation at different incident angles indicates a need for wavelength calibration after an AOTF is positioned for use in a spectrophotometer.

Wavelength/Bandpass Relationship. The bandpass of the light diffracted by an AOTF varies with its wavelength in accord with Eq. 2. To measure the resolution of our device, we used the experimental arrangement described in Fig. 1. The slit widths of the 1 monochromator were set at 50 μm. The bandpass of the monochromator (0.04 nm) was much smaller than the resolution expected from the AOTF, ensuring that the measured spectral bandpass was a function of only the AOTF output. In Fig. 7, the FWHM is plotted with the corresponding wavelength squared. The bandpass of the AOTF ranged

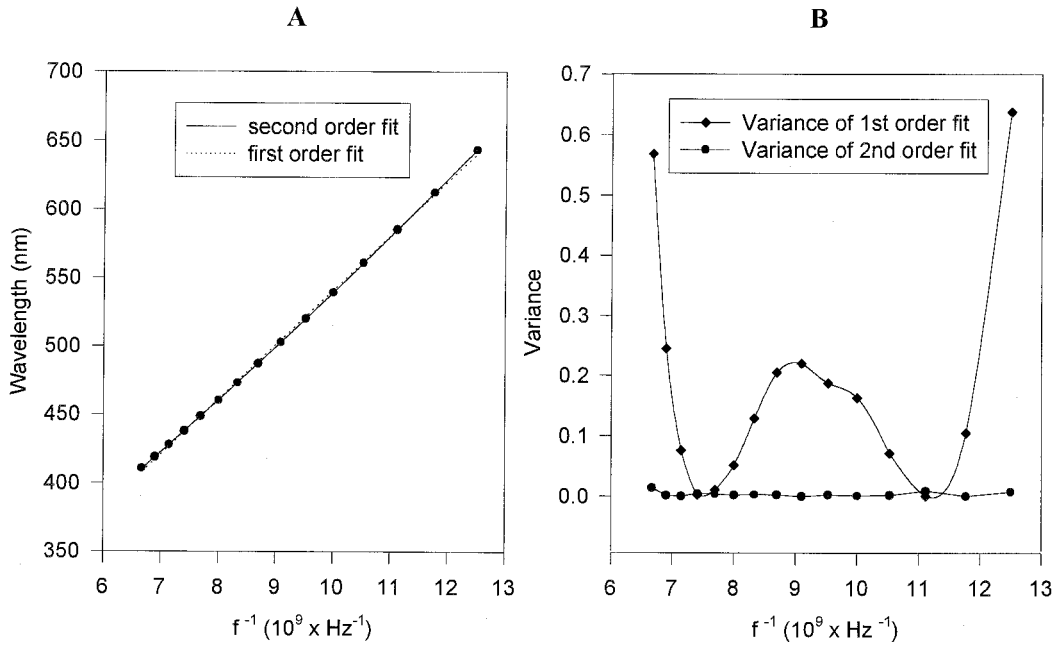

FIG. 5. (**A**) Relationship between the output wavelength and the applied frequency. (**B**) Variance in the output wavelength and the calculated values based upon linear and second-order functions.

from 0.82 nm (at 150 MHz, which corresponds to 410.8 nm) to 2.64 nm (at 80 MHz or 643.6 nm). The relationship is linear ($r^2 = 0.990$) and in agreement with Eq. 2. As expected, the resolution of an AOTF is better at a shorter wavelengths.

The measured resolution of our device is similar to the bandpass of the paratellurite devices used by Fulton and Horlick.[8] They studied spectral resolution by observing separation of peaks in hollow cathode lamps spectra. In their work, two neon lines at 375.13 and 375.42 nm ($\Delta\lambda = 0.30$ nm) could be distinguished; however, in the 641 nm region, peaks had to be 1.9 nm apart to be differentiated (Ne lines at 640.23 and 638.30 nm). The resolution of a paratellurite AOTF is sufficient for many molecular spectroscopy applications and some applications involving atomic spectrometry.

Preliminary Results of AOTF Applications to Visible Spectrophotometry. *Wavelength Calibration.* Following the fundamental characterization of the AOTF as a monochromator device, it was inserted into the spectrophotometer configuration shown in Fig. 2. To perform wavelength calibration with the present incident angle and configuration, we took advantage of the spectroscopy of rare earth elements. Some of these elements exhibit sharp absorption features in the visible spectral region that make the wavelength assignment easy and precise. To perform the calibration of the spectrophotometer, we obtained spectra of holmium, praseodymium, and niobi-

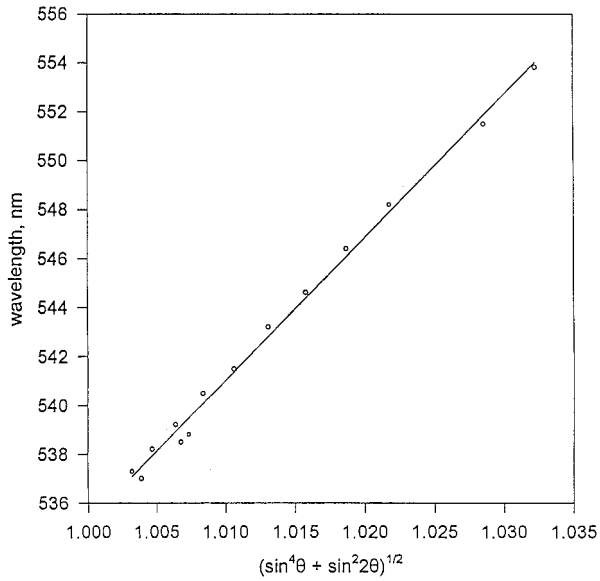

FIG. 6. Output wavelength as a function of incidence angle.

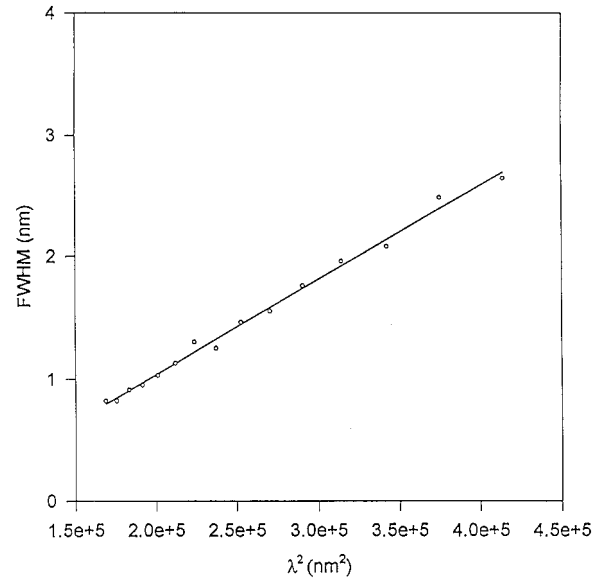

FIG. 7. Bandpass as a function of output wavelength.

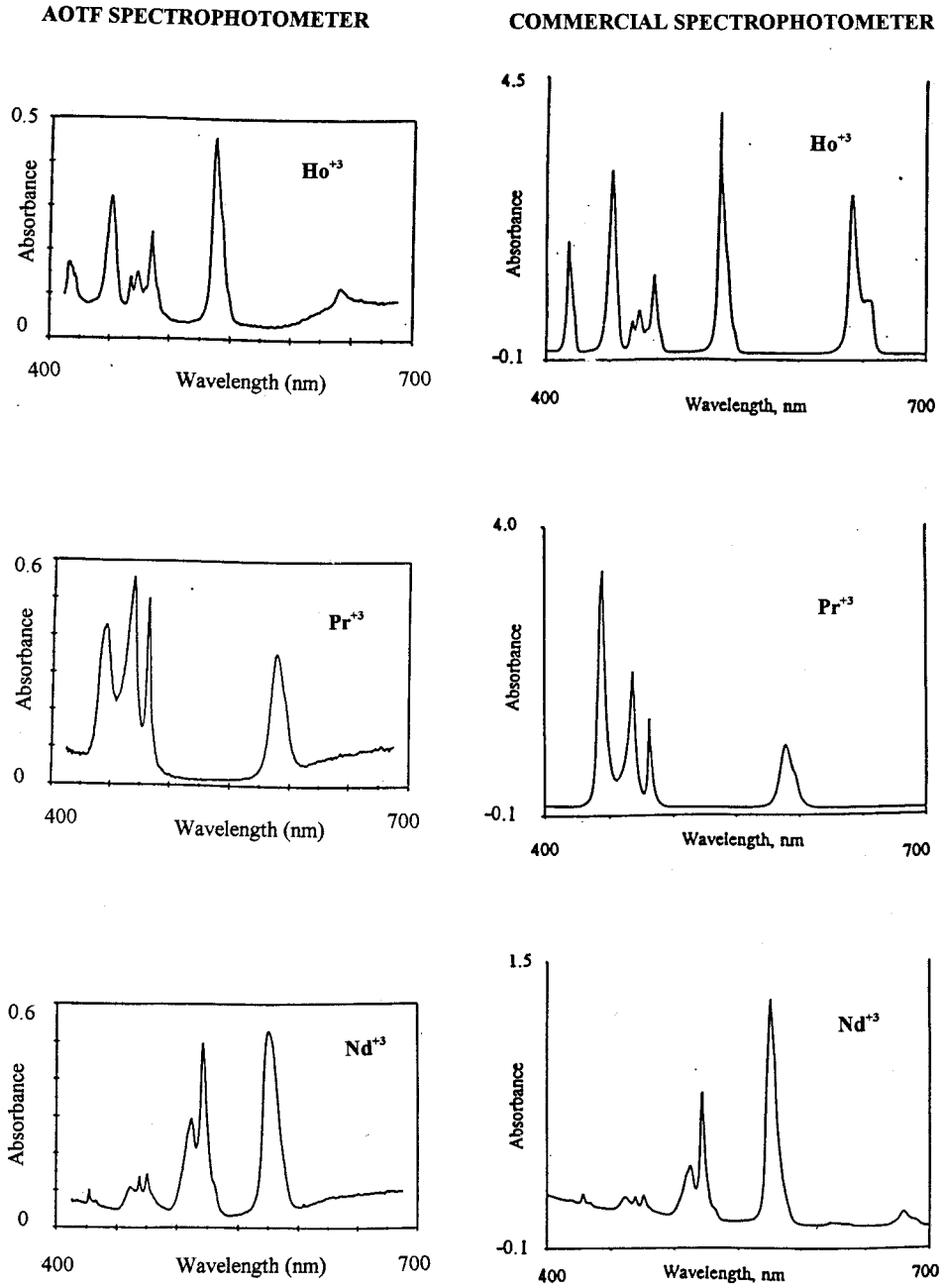

FIG. 8. Spectra of holmium, praseodymium, and neodymium perchlorates obtained with the Varian 2290 and the AOTF spectrophotometers.

um perchlorates (see Fig. 8). Each spectrum was calculated on the basis of three measurements: the spectrum of a sample, a blank (establishing 100% T), and the spectrum registered with the light blocked (0% T). In the initial spectra, the absorbance was plotted vs. inverse of frequency, as the wavelength of the diffracted light is proportional to the inverse of applied frequency (see Eq. 1). The frequencies of the spectral peaks for the same solutions were then correlated with the wavelengths of the maximum absorption determined on the Hitachi U-3410 spectrophotometer. The wavelength calibration plot, based on sixteen data points, is presented in Fig. 9. As during the initial characterization of the AOTF, described in the previous section, the second-order fit correlates the data best ($r^2 = 0.99994$) and was used for the calibration of the spectrophotometer.

Spectral Characteristics of the AOTF Spectrophotometer. The spectra of three rare earth elements obtained with both the AOTF and the commercial spectrophotometer are presented for comparison in Fig. 8. The shape of the peaks and the wavelengths of the absorption maxima correlate very well, although the AOTF spectra have nonzero absorbance in the regions where, according to the results from the commercial instrument, the compounds should not absorb. This observation is probably the effect of the presence of scattered light in the AOTF spectrophotometer.

There is a noticeable difference in the relative intensity of some peaks. This effect is caused, in part, by the fact that AOTF efficiency is dependent on the incident angle. The upper two holmium perchlorate spectra in Fig. 10 were taken at different incoming light angles and show

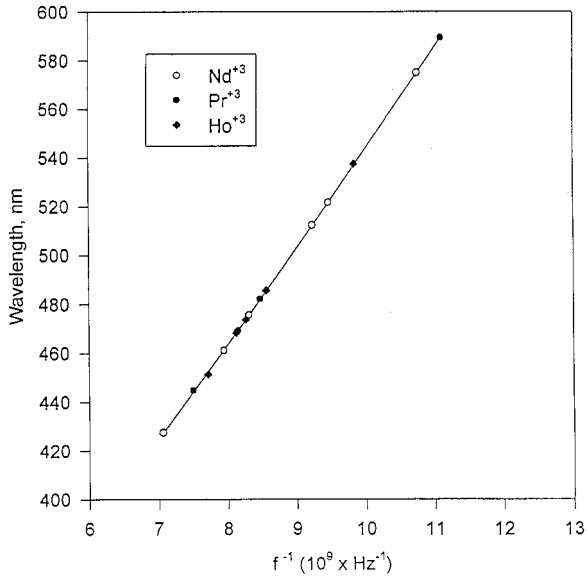

FIG. 9. Wavelength calibration of the AOTF spectrophotometer.

significant differences in the relative intensities of absorption bands. In spectrum **A**, the peaks in the lower range (below 500 nm) have intensities similar to the bands in the spectrum registered with a commercial instrument (spectrum **C**). However, the band at about 640 nm is much less intense compared to the peak in spectrum **C**. The opposite effect can be seen in spectrum **B**, where the intensity of the band at 640 nm is enhanced but features in the region between 400 and 500 nm are suppressed. The strong dependence of the spectral intensity on the angle between the incoming light and the AOTF indicates the need for experimental determination of an optimal position of the crystal and minimization of stray light in the spectrophotometer.

As can be expected, because the incident angle was changed during these two measurements, the peak positions in the spectra changed slightly. The most intense peak in the spectrum at 537.3 nm occurs at 101.63 MHz (0.00984 MHz^{-1}) in spectrum **A** but is shifted to 101.11 MHz (0.00989 MHz^{-1}) in spectrum **B**. Similarly, the second most intense maximum at 541.4 nm that appears at 130.04 MHz (0.00769 MHz^{-1}) in spectrum **A** is shifted about 0.84 MHz to 129.20 MHz (0.00774 MHz^{-1}) in spectrum **B**. The approximate peak shifts were about 1.5 nm. This effect has been compensated by calibration with the use of the known absorbance peaks of holmium(III).

Detector Response and the Stray Radiation. It is likely that the "nonzero" absorbances in the AOTF spectra at wavelengths that exhibited zero absorbance with the commercial instrument were caused by nonmonochromatic radiation. It is likely that scattered light and deviations from perfect monochromatic AOTF output are the sources of this nonmonochromatic radiation. For these examinations, we obtained a spectrum of 0.22 M cobalt perchlorate solution under a variety of conditions. As shown in the spectrum obtained with the commercial instrument (Fig. 11A), cobalt perchlorate has a broad absorption spectrum with a maximum at 510 nm. The spectrum presented in Fig. 11B was recorded by using the AOTF spectrophotometer with a 1P28 PMT as a detector,

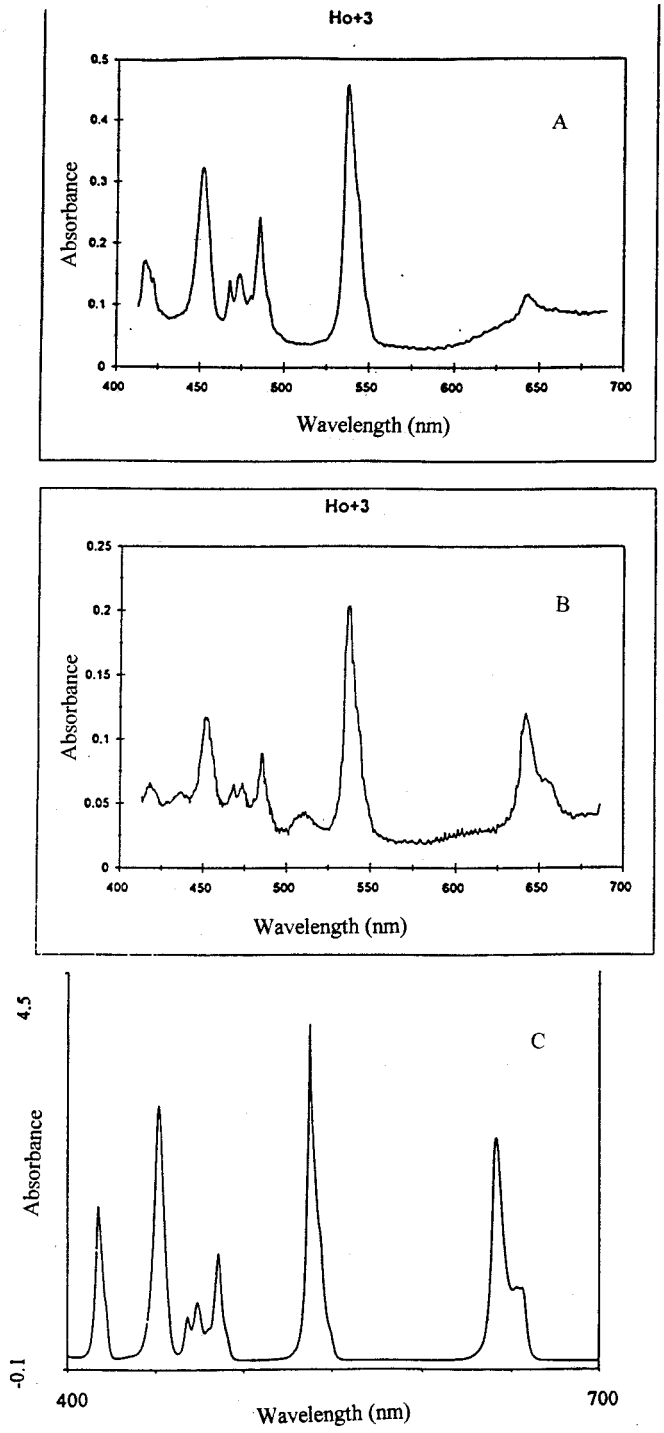

FIG. 10. Comparison of holmium spectra obtained with two different AOTF incident angles (**A** and **B**) and with the Hitachi U-3410 spectrophotometer (**C**).

while the multialkali R955 PMT was used to record the spectrum in Fig. 11C. Figures 11D and 11E present the PMT signals for the perchloric acid solution blank (the bottom curve) and the sample (the top curve) for the 1P28 and the R955 photomultiplier tubes, respectively.

The general shapes of the spectra in Figs. 11A, 11B, and 11C are similar. However, there is a significant difference in the 690 to 590 nm range in spectrum **B** with the 1P28 PMT. This region shows an increase in the ab-

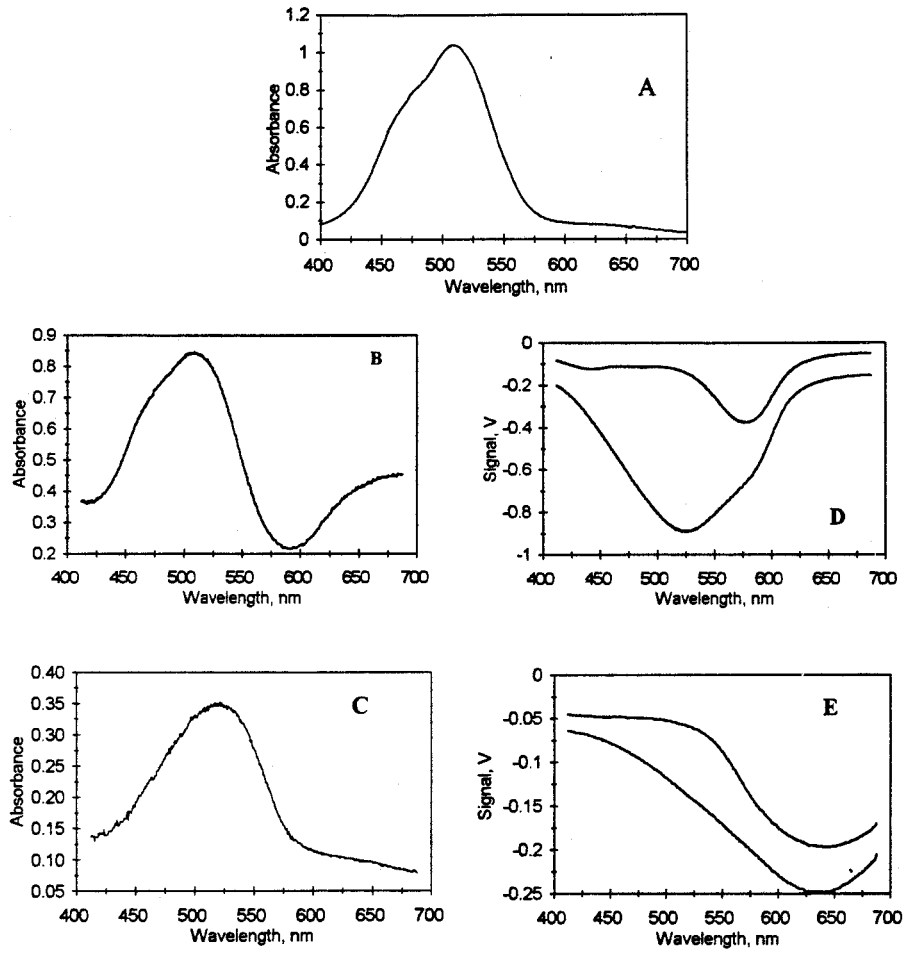

FIG. 11. Cobalt absorbance data. (**A, B**, and **C**) Absorbance spectra obtained with the Varian 2290 spectrophotometer and the AOTF spectrophotometer with the 1P28 and R955 PMTs, respectively. (**D** and **E**) AOTF spectrophotometer detector outputs with analyte-containing and solvent-only solutions with the 1P28 and R955 PMTs, respectively. The zero y-values on Figs. **D** and **E** indicate the voltage output when the radiation is blocked (corresponding to 0% transmittance).

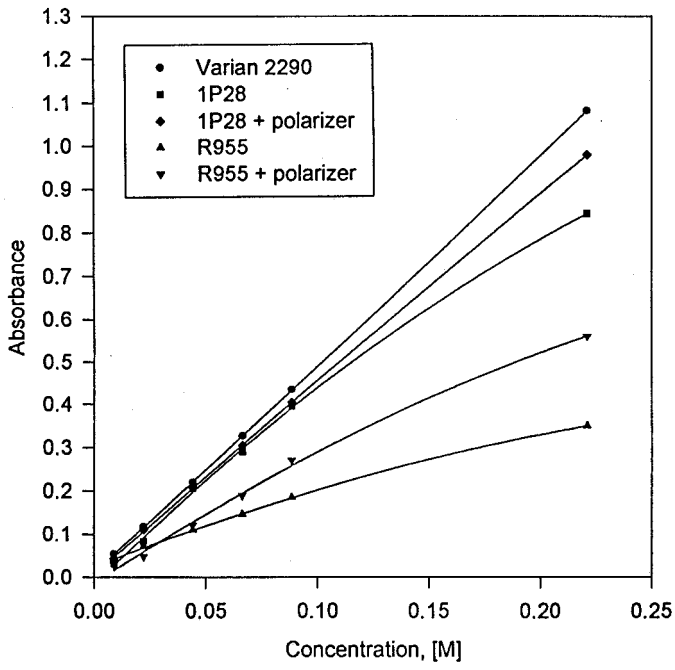

FIG. 12. Calibration plots for 510 nm cobalt obtained with the AOTF spectrophotometer with the R955 and 1P28 PMTs.

sorption, which does not appear in the spectrum acquired with the R955 PMT or the commercial instrument. The reasons for the differences between spectra **B** and **C** reside in the response characteristics of the two photomultiplier tubes. As Figs. 11D and 11E show, the best response for the 1P28 PMT occurs at about 525 nm, where the signal is the largest, but the R955 PMT responds the best at much longer wavelengths (about 630 nm). Therefore, the scattered light influences the spectrum to a much larger extent at the longer wavelengths when the 1P28 PMT is used as a detector in the spectrophotometer, because the amount of light registered by the PMT is much smaller. In contrast, the R955 photomultiplier tube does not respond well in the mid-range of the spectrum.

Calibration plots for cobalt perchlorate solutions are presented in Fig. 12. The calibration curve determined with the commercial instrument show an excellent linearity in the range of concentrations tested, with the slope of 4.8 absorbance units/M. Because the 510 nm wavelength is in the region where the response of the 1P28 PMT is better than the R955 PMT, the curve determined with the R955 PMT is much more affected by the scattered light and shows a larger deviation from linearity. Both curves are linear up to about 0.09 M and show "roll overs" at higher concentrations. The slope of the plot

obtained with the 1P28 PMT is larger than the slope of the R955 PMT curve (3.0 vs. 1.8 absorbance units/M).

It was possible to reduce the amount of scattered light by polarizing the white light. This phenomenon can be predicted theoretically, since the AOTF device diffracts light of only one polarization. Light of any other polarization can contribute only to nonmonochromatic light effects. A sheet polarizer was placed between the tungsten lamp and the AOTF in the spectrophotometer, as shown in Fig. 2. The polarizer was rotated so that only light of the proper orientation for AOTF diffraction was allowed to traverse the system. The calibration plots obtained with the polarizer in the light path are shown in Fig. 12. The deviation from the plot determined with the commercial instrument is much smaller compared to the calibration curves registered without the polarizer. The R955 PMT calibration curve with the polarizer ''rolls over'' at concentrations higher than 0.09 M and has a slope of 3.1 absorbance units/M. The curve registered with the 1P28 PMT is linear over the entire range of concentrations (up to 0.22 M) with a slope of 4.5 absorbance units/M, only slightly smaller than the slope of the curve obtained with the commercial instrument (4.7 absorbance units/M). Similar effects were observed when calibrations for potassium permanganate and holmium perchlorate were obtained.

CONCLUSION

Because of their small size, solid-state nature, relatively low cost, and spectral behavior, AOTFs exhibit the potential for widespread spectrometry applications. The initial characterization of the paratellurite acousto-optic device showed that it can be used as a spectrophotometer monochromator in the visible range of the spectrum. The wavelength of the diffracted light can be rapidly changed by varying the frequency of the acoustic wave in the microsecond time scale. In our study the entire spectrum was scanned continuously, and random wavelength access can be achieved. The bandpass of an AOTF depends on the wavelength of the diffracted light. For the device studied in this paper, the bandpass was determined to be 2.5 nm at 633 nm and 0.5 nm at 400 nm. These values are quite satisfactory for many types of spectroscopic measurements. Better resolution can be expected in the UV range.

The initial results of the application of the AOTF to a visible spectrophotometer are encouraging. The spectra obtained with the AOTF spectrophotometer have absorption bands of the same shape and wavelength as the spectra recorded with commercial instruments. The relative intensity of the peaks may vary, but this factor should not be a significant barrier for the implementation of the new device. The next challenge is to improve the performance of the spectrophotometer by reducing the fraction of nonmonochromatic light.

ACKNOWLEDGMENT

We gratefully thank the E. L. Ginzton Research Center, Varian Associates, Incorporated, for their financial support of this project.

1. C. D. Tran, Anal. Chem. **64,** 971A (1992).
2. J. Lekavich, Lasers & Applications **59** (1986).
3. J. Xu and R. Stroud, *Acousto-Optic Devices. Principles, Design, and Applications* (John Wiley and Sons, New York, 1992), Chap. 7.
4. A. Korpel, *Acousto-Optics* (Marcel Dekker, New York, 1988).
5. A. P. Goutzoulis, and D. R. Rape, *Design and Fabrication of Acousto-Optic Devices* (Marcel Dekker, New York, 1994), Chap. 4.
6. C. D. Tran and J. Lu, Anal. Chim. Acta **314,** 57 (1995).
7. D. P. Baldwin, D. S. Zamzow, and A. P. D'Silva, Appl. Spectrosc. **50,** 498 (1996).
8. G. Fulton and G. Horlick, Appl. Spectrosc. **50,** 885 (1996).
9. C. D. Tran and J. Lu, Appl. Spectrosc. **50,** 1578 (1996).
10. C. D. Tran and R. J. Fulran, Anal. Chem. **65,** 1675 (1993).
11. C. D. Tran and R. J. Fulran, Anal. Chem. **64,** 2775 (1992).
12. E. N. Lewis, P. J. Treado, and I. W. Levin, Appl. Spectrosc. **47,** 539 (1993).
13. C. D. Tran and G. H. Gao, Anal. Chem. **68,** 2264 (1996).
14. J. F. Turner II and P. J. Treado, Appl. Spectrosc. **50,** 277 (1996).
15. P. J. Treado, I. W. Levin, and E. N. Lewis, Appl. Spectrosc. **46,** 1211 (1992).
16. P. J. Treado, I. W. Levin, and E. N. Lewis, Appl. Spectrosc. **46,** 553 (1992).
17. F. Moreau, S. M. Moreau, D. M. Hueber, and T. Vo–Dinh, Appl. Spectrosc. **50,** 1295 (1996).
18. C. D. Tran and V. Simianu, Anal. Chem. **64,** 1419 (1992).